JAAS FULL PAPER
www.rsc.org/jaas

Application of a multi-way method to study long-term stability in ICP-AES†

Ana Marcos, Michael Foulkes and Steve J. Hill*

Department of Environmental Sciences, Plymouth Environmental Research Centre, University of Plymouth, Drake Circus, Plymouth, UK PL4 8AA

Received 31st October 2000, Accepted 13th December 2000
First published as an Advance Article on the web 31st January 2001

Although major advantages have been made in developing robust, easy-to-use ICP-AES instruments offering sub μg g^{-1} detection limits and relative interference free operation, long-term drift of the analytical signal continuous to be problematic and necessitates regular re-calibration. The work presented here focuses on the effect of two instrumental parameters, *i.e.* the rf power and the nebuliser gas flow rate, on the robustness of the signals. The effects on the long-term stability when varying these two factors was systematically studied using an experimental design protocol. A "*drift diagnosis*" on thirty emission lines was performed at 12 different sets of operating conditions by repeated determination of a multi-element solution over several hours. The results were studied using standard parameters, *i.e.*, Mg ratio, sensitivity, drift error, drift patterns and multi-way analysis. Parallel factor analysis (PARAFAC) was employed to analyse the 3-way data array *generated*: "*emission lines* × *replicates* × *operating conditions*". The physical interpretation of the new PARAFAC-factors is shown to enable a better understanding of the drift phenomenon by mathematically characterising the causes of long-term instability. Finally, the robustness of the technique using different operating conditions is evaluated and the appropriate use of internal standards to correct for drift is discussed.

Introduction

Inductively coupled plasma atomic emission spectrometry (ICP-AES) is a well established technique for routine analysis.[1] Multi-element determinations, high selectivity and limits of detection below the μg g^{-1} level have led to a wide range of applications in the areas of food sciences, environmental and clinical analysis. Although most of the disadvantages once associated with ICP-AES have now been well characterised and can often be eliminated, long-term stability phenomenon may necessitate the analyst to recalibrate the instrument at regular intervals.

The causes of such instability are not fully understood. Initial studies[2–8] have identified the presence of flicker noise, mainly related to the sample introduction system, as the origin of the problem, *i.e.*, long-term instability is caused by slight fluctuations in the instrumental parameters. Further work[6,9] identified three areas of instability: variation of the nebulisation efficiency; changes in the energy transfer from the plasma to the sample; and degradation of the optics system. In many modern instruments, software routines control the stability of the optical system and allow it to be monitored during the analysis. However, the operator usually has little or no information about the state of the sample transport system nor the stability of the plasma. The objective of this study was, therefore, to better characterise the drift phenomena by studying the two instrumental parameters most likely to have an effect on these parts of the system. The nebuliser gas flow rate and the rf power were chosen since these two settings are directly related to the nebulisation process and the energy transfer.

To carry out the study, the evolution of emission signals with time at different rf powers and nebuliser gas flow rates was monitored. In order to approach the problem in a systematic way, the selection of the instrumental settings was achieved using an experimental design protocol. The robustness of the technique at different operating conditions is evaluated using standard parameters: long-term error, drift patterns, magnesium ratio[10,11] and correlation degrees[12] to identify similarities and differences between the emission lines *i.e.*, analyte and argon lines, atomic and ionic emission lines. However, for data handling purposes, a multi-way approach[13] was necessary to facilitate the three dimension structure of the results. Our data can be arranged in a cubic array, indexed: emission lines × replicates × instrumental conditions.

A multi-way decomposition method, parallel factor analysis, PARAFAC,[14,15] was then performed on the data set. Two PARAFAC-factors were calculated and their physical relevance investigated in terms of energy data, drift patterns and instrumental conditions.

Background

In essence, six parameters need to be set before running an ICP-AES analysis: the three argon flows (plasma, nebuliser and auxiliary flow), the sample uptake rate, the rf power and the viewing height. In addition to these, the size of the entrance slit, the integration time and the type of background correction employed will determine the nature of the mathematical process used to convert the raw signal into usable data. When trying to identify the effect of small variations in the instrumental parameters on the signals, there is a problem in isolating each function since the working parameters are interrelated. For instance, an increase in the nebuliser flow rate may improve the transport efficiency by creating a finer aerosol, such that more drops will reach the plasma, and thus the intensity of the signal could be enhanced. However, at the same time, a higher nebuliser flow will decrease the residence time of the sample aerosol in the plasma, so that less energy will be transferred to the sample, with the potential loss of some emissions lines. Although the transport of the sample to the plasma will be largely influenced by the sample uptake rate and

†Electronic Supplementary Information available. See http://www.rsc.org/suppdata/ja/b0/b008759i/

the nebuliser gas flow rate, other factors will also have an effect on the type of aerosol created, *e.g.*, the viscosity of the sample, type of nebuliser and spray chamber employed, as well as the room temperature. In terms of energy transfer, the instrumental parameters with most influence are the rf power supply, the three argon flows and the sample uptake rate. Since these instrumental parameters are interrelated, a systematic study of the influence of the variation of each parameter on the robustness of the emission signal would lead to a high number of experiments. For example, if the six instrumental parameters mentioned above (*i.e.*, rf power, sample uptake rate, the three argon flows and the viewing high) are considered for just two different settings of each parameter, 64 experiments would be required to study all the interactions. For this reason, we have limited the number of instrumental parameters to be modified to the rf power and the nebuliser gas flow rate.

The power delivered to the plasma will determine its temperature, with higher power resulting in higher temperatures. Higher temperatures enhance emission for all ionic lines, however, the effect on atomic lines depends on the relative excitation and ionisation energies of the emitting atom: short wavelengths atomic lines are enhanced; long wavelength atomic lines are suppressed; and moderate wavelength atomic lines remain relatively unaffected.

The nebuliser flow affects the average size of the aerosol droplets, but also the residence time of the sample in the plasma and the plasma temperature. At low nebuliser flow, the average size of the aerosol droplets increases, reducing the transport efficiency of the spray chamber. Thus, every line will partially decrease its emission intensity as less sample reaches the plasma. However, a lower nebuliser flow will also increase the residence time of the aerosol in the plasma and the plasma temperature. This could enhance the emission of any ionic line. For atomic lines, the increased residence time provides energy to promote two competing pathways: the excitation, which leads to emission enhancement, and ionisation, which leads to emission suppression. Therefore the net effect will depend on the relative energies of the two processes such that: (1) high-energy atomic emission lines emitted by elements that resist ionisation (*e.g.*, Zn) show enhanced emission with increased residence time; (2) low-energy atomic emission lines emitted by elements that are easily ionised (*e.g.*, Na) show suppressed emission with increased residence time; and (3) moderate-energy atomic emission lines emitted by atoms of moderate ionisation energy (*e.g.*, Cu) remain unaffected by residence time.

Clearly, even when considering only two factors, an ICP is a complex system and, for this reason, a systematic approach to the problem is essential. We have used an experimental protocol to plan our experiments. The experimental design strategy[16,17] gathers together experimental knowledge. It can be applied to investigate a phenomenon in order to gain further understanding or to improve performance. When planning experiments, the influence of different parameters can be studied simultaneously. In this study the experimental design was used to evaluate the effect of each instrumental parameter individually as well as the interactions between them.

The *N*-way approach: PARAFAC

Many analytical chemist have introduced multivariate methods such as principal component analysis (PCA), principal component regression (PCR) or partial least squares (PLS) to further study their results.[18] In standard multivariate analysis, data are arranged in a two-way structure, a table or a matrix. An example could be a data matrix which has different samples along the rows with the concentration of several elements along the columns. However sometimes, a third dimension is necessary to describe the data. Consider for instance, using the example above, the determination of a number of metals in various samples and at different pH. Such data could be arranged in a three-way structure, indexed by sample, element and pH.

In this study, we have produced data matrices in which each row represents an emission line and each column a replicate of its intensity over time. As we repeat the experiment under different working conditions, we can arrange all the data in an array, a cube of data, indexed by line, replicate and experiment (Fig. 1). In such a cube, one dimension will contain the different emission lines, the second dimension the replicates and the third dimension the different experimental conditions employed. We therefore produce a 3-way data set and, thereby, multi-way methods can be applied.

We have employed PARAFAC[14] (parallel factor analysis) to describe the data. Although PARAFAC was originally employed in psychometrics,[19] several applications of PARAFAC in chemical systems have been reported. Most of them corresponded to decomposition processes in excitation–emission fluorescence spectroscopy for data treatment[20,21] and also for instrument optimisation.[22] Applications of PARAFAC to high-performance liquid chromatography (HPLC) coupled with different detectors[23,24] have also been found. Applications in the chemical industry have also been reported.[25–27]

PARAFAC is a decomposition method for 3 or higher orders arrays, which could be compared to principal component analysis (PCA). The aim of decomposition is to retain the maximum amount of information from the data but represent it in a smaller number of components or factors. Using PARAFAC, instead of working with a 2-way data set, the algorithm is extended to higher modes, 3, 4 or in general *N*-way data sets. The structural model of a two-way PCA is a bilinear model [eqn. (1)], and likewise a PARAFAC model of a three-way array is defined by the structural model described in eqn. (2):[14]

$$x_{ij} = \sum_{f=1}^{F} a_{if} b_{jf} + e_{ij} \quad (1)$$

$$x_{ijk} = \sum_{f=1}^{F} a_{if} b_{jf} c_{kf} + e_{ijk} \quad (2)$$

where x_{ijk} represents data in object i of variable j at condition k; i,j,k are variables respectively along the first, second and third dimension (Objects, Variables, Conditions); f, F are principal components or factors; a,b,c is the model loading on first, second and third dimension; and e is the model error.

A decomposition of the data is made into triads or trilinear components. The results of a PARAFAC analysis are given as *N*-loading matrices, one for each mode studied. In our case, we are dealing with a three way data set, and three loading matrices will be obtained A, B and C. The trilinear model is found to minimise the sum of squares of the residuals e_{ijk} in the model. Eqn. (2) may be represented graphically as in Fig. 2.

It should be stressed that the reason for using a multi-way method is not to obtain a better fit for the data, but rather more adequate, robust and interpretable models, based on a smaller number of parameters. For example, in order to calculate an F-component PCA model to a $I \times J \times K$ array, we would need first to unfold the data to a $I \times JK$ matrix and then apply a PCA, the solution of which will consist of $F(I+JK)$ parameters

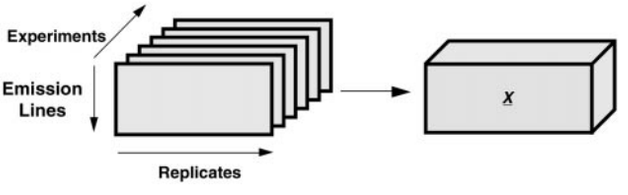

Fig. 1 3-Way arrangement of data sets.

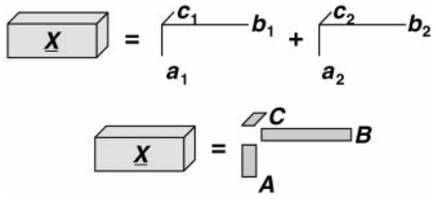

Fig. 2 Geometrical representation of a PARAFAC analysis.

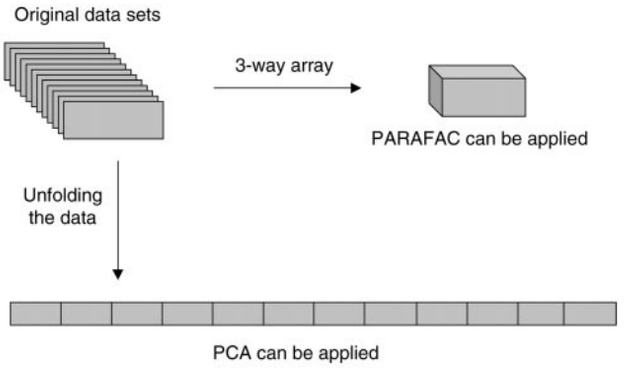

Fig. 3 Differences in the data disposition to perform a PARAFAC or a PCA.

(Fig. 3). A corresponding PARAFAC model with an equal number of components would consist of only $F(I+J+K)$ parameters. Clearly the PCA model will be more difficult to interpret because a much higher number of parameters are implied. In our case, we are dealing with an array of *30 emission lines × 100 replicates × 12 instrumental conditions. Each PARAFAC factor will be defined by (30+100+12)→**142 parameters***.

If we want to explain the same data set by a PCA, we first need to unfold the data sets to a matrix which dimension will be *30 emission lines × (100 replicates × 12 instrumental conditions) giving 30 emission lines × 1200 variables. Each PCA factor will be defined by (30+1200)→**1230 parameters.***

Another advantages of PARAFAC *versus* unfolded PCA is the uniqueness of the solution. In bilinear methods, the solutions present rotational freedom. This is not the case with PARAFAC, where the estimated model cannot be rotated without a loss of fit.

Experimental

Methodology

To generate the data set, a multi-element solution (10 μg g^{-1}) containing 15 analytes (see Table 1) was repeatedly analysed over a period of 8 h without recalibration. In order to ensure stable starting conditions, 2 h were allowed to warm up the instrument prior to starting the measurements. The evolution of the intensities from 30 emission lines was then followed over time. The lines studied are reported in Table 1 and represent one atomic and one ionic line for most elements and four argon lines.

Instrumentation

The instrument employed was an Optima 3000 (Perkin-Elmer Corporation, Norwalk, USA). This ICP-AES instrument combines an echelle polychromator with a solid state detector which allows simultaneous acquisition of over 5000 lines with simultaneous background measurements. The instrumental parameters employed are shown in Table 2. The settings for the nebuliser gas flow rate and rf power were defined using an experimental design.

Table 1 Emission lines used in this study

Element	λ/nm	Intensity I_n/I_b [a]	EE[b] = λ/eV	IP[c]/eV	EP + IP[d]/eV
Al (I)	396.152	10.5	3.13	—	3.1
Ba (II)	230.424	73.0	5.38	5.21	⩾10.6
Ba (II)	233.527	75.0	5.31	5.21	11.2
Ca (I)	422.673	1.5	2.99	—	2.9
Ca (II)	317.933	1.5	3.90	6.11	13.1
Cd (I)	228.802	110	5.42	—	5.4
Cd (II)	226.502	120	5.47	8.99	14.4
Co (I)	340.512	NO DATA	3.64	—	4.0
Co (II)	228.616	43.0	5.42	7.88	14.3
Cr (I)	357.869	13.0	3.46	—	⩾3.46
Cr (II)	267.716	42.0	4.63	6.77	⩾11.4
Cu (I)	324.754	56.0	3.82	—	3.8
Cu (II)	224.700	39.0	5.52	7.73	15.9
Fe (II)	259.940	48.0	4.77	7.90	⩾12.7
Mg (I)	285.213	NO DATA	4.35	—	4.3
Mg (II)	279.079	1.0	4.44	7.65	⩾12.1
Mn (I)	403.076	6.8	3.08	—	3.1
Mn (II)	257.610	220	4.81	7.43	12.2
Na (I)	589.592	43.0	2.10	—	2.1
Ni (I)	232.003	20.0	5.34	—	⩾5.34
Ni (II)	231.604	15.0	5.35	7.64	⩾13.0
Pb (II)	220.353	70.0	5.62	7.42	14.7
Ti (II)	379.280	NO DATA	3.27	6.83	⩾10.1
Zn (I)	213.856	170	5.80	—	5.8
Zn (II)	202.548	75.0	6.12	9.39	15.5
Ar (I)	357.229	2.3	3.47	—	⩾3.47
Ar (I)	404.597	2.5	3.06	—	⩾3.06
Ar (I)	420.068	50	2.95	—	⩾2.95
Ar (I)	451.074	21	2.75	—	⩾2.75

[a] I_n/I_b Ratio of net analyte intensity to background intensity (from Handbook of ICP-AES, CRC Press, 1981). [b] EE Transition emitted energy (calculated converting the nm^{-1} to eV). [c] IP First ionisation potential (from Handbook of Physics and Chemistry, CRC Press, 77th Edition, 1997). [d] EP + IP Excitation potential (Handbook of Spectroscopy Vol.1, PW Robinson CRC Press, 1974).

Table 2 Instrumental settings used in experimental work

Rf power	Designed variable
Injector diameter	2 mm
Nebuliser type	Cross flow pneumatic nebuliser
Nebuliser flow	Designed variable
Plasma flow	15 l min^{-1}
Auxiliary flow	0.8 l min^{-1}
Sample uptake rate	1.0 l min^{-1}
Viewing height	12 mm
Read time	10–20 s

Experimental design settings

A combination of two full-factorial designs was employed: a full-factorial experiment of two factors at three levels (Table 3) → ***9 experiments***; and a full-factorial experiment of two factors at two levels (Table 4) → ***4 experiments***.

The centre conditions (*point (0,0): rf power 1250 W and nebuliser flow rate 0.9 l min^{-1}*) were replicated three times. A graphic representation of the experimental points is shown in Fig. 4. In total, 15 experiments were planned and, for each experimental point, a data set was produced, *i.e.*, the intensity of the selected emission lines was measured 99 times (approximately 8 h).

An overview of the final experimental protocol is presented in Table 5. The robustness of the instrument at the different instrumental conditions employed is also reported on Table 5. The robustness of the plasma is referred to[28] as "*its ability to keep the variation of the analytical signal to a minimum when changing the sample matrix*". To quantify robustness, Mermet[11] introduced the magnesium ionic-to-atomic line intensity ratio where values over 10 provide a robust plasma, whilst a Mg ratio below 10 indicates that any changes in the sample matrix would highly affect the emission intensities. Although in this work we have not matched the test solution with a complex chemical matrix to simplify the problem, the Mg ratio at each instrumental setting was determined to provide an additional factor to evaluate the operating conditions selected for this study.

N-way data handing

Matlab software (Mathworks, Inc.; Version 5.1) and the *N*-Way Toolbox for Matlab[29] were employed to perform the 3-way analysis. Before running a PARAFAC analysis, the data was scaled to unit squared variation. Scaling in multi-way analysis has to be done taking the trilinear model into account. If variable *i* of the first mode is to be scaled (compared to the rest of the variables in the first mode), it is necessary to scale all rows where variable *i* occurs by the same scalar. This means that whole matrices instead of rows were scaled. Mathematically scaling within the first mode can be described as:

$$x_{ijk}^{\text{scal}} = \frac{x_{ijk}}{\boldsymbol{S}_i} \tag{3}$$

Where S_i will scale to unit squared variation:

$$S_i = \sqrt{\left(\sum_{j=1}^{J}\sum_{k=1}^{K} x_{ijk}^2\right)} \tag{4}$$

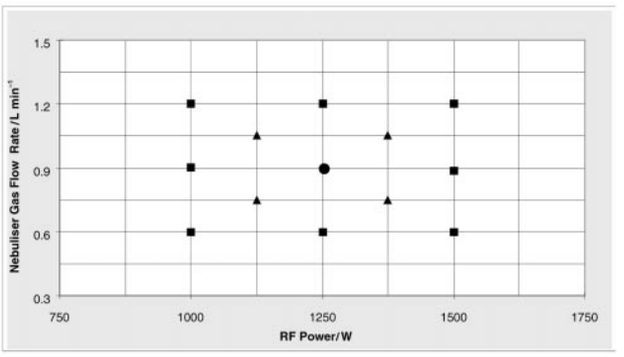

Fig. 4 Graphical representation of the experimental design.

Table 3 Experimental designed levels, block 1

Factor 1			Factor 2		
Rf power/W			Nebuliser flow rate/l min^{-1}		
−1	0	+1	−1	0	+1
1000	1250	1500	0.6	0.9	1.2

Table 4 Experimental designed levels, block 2

Factor 1		Factor 2	
Rf power/W		Nebuliser flow rate/l min^{-1}	
−0.5	+0.5	−0.5	+0.5
1125	1375	0.75	1.05

The core consistence and the explained variance were the two parameters employed to optimise the number of components to use in the PARAFAC model. The core consistence diagnosis is a percentage below or equal to 100%. A value of 80–100% means that the model is valid, while a value below 40% means that the model is not valid. A core consistency between 40 and 80% means that the model is probably valid but somehow difficult to estimate, *e.g.*, due to slight mis-specification or high correlation. The core consistency may decrease with the number of components, but very sharply where the correct number of components is exceeded. Hence, the appropriate number of components is the model with the highest number of components, highest explained variation and a valid core consistency. Four PARAFAC models were calculated using one, two, three and four components. The explained variance increased continuously with the number of components, see Fig. 5(A). The core consistency fell to values around 10%, when more than two components were calculated, Fig. 5(B). Therefore, a two components PARAFAC model was employed in this analysis.

Table 5 Experiment plan

Experiment	Rf power/ W	Nebuliser flow rate/ l min^{-1}	Room temperature/ °C	Magnesium ratio (MgII/MgI)
Central conditions (1)	1250	0.90	26–27	10.5
Experiment 1	1125	1.05	27.5–28.5	8.9
Experiment 2	1125	0.75	28	8.4
Experiment 3	1375	1.05	29.5–29	10.9
Experiment 4	1375	0.75	28.5–29.5	11.1
Central conditions (2)	1250	0.90	28.5–27	10.5
Experiment 5	1000	0.90	26	6.7
Experiment 6	1250	1.2	26–26.5	8.6
Experiment 7	1250	0.6	26–25	10.1
Experiment 8	1500	0.9	25–25.5	12.5
Central conditions (3)	1250	0.90	24.5–24	10.5
Experiment 9	1000	1.2	23–26	5.8
Experiment 11	1500	1.2	25–26.5	10.3
Experiment 12	1500	0.6	26–28	11.6

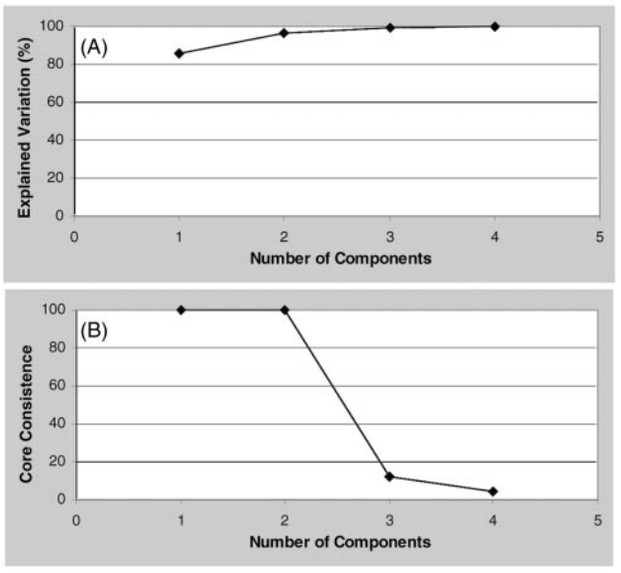

Fig. 5 Optimisation of the number of PARAFAC components. (A) Variance explained depending on the number of components and (B) core consistencies depending on the number of components.

Results and discussion

Classical analysis

One data set was obtained for each experiment with the exception of where the experimental conditions were such that the plasma could not be sustained, *i.e.*, rf power 1000 W and nebuliser gas flow rate 0.6 l min^{-1}. As expected, the intensity levels of every line changed from one set of experimental conditions to another, and so did the sensitivity. Table 6 shows the limits of detection for every line at the different operating condition selected for this study and reflects a degradation of sensitivity when robust conditions are employed, and more precisely when low nebuliser flows are set.

In order to check the stability of the instrument from one day to another, an intensity check using the central conditions (rf, 1250 W; nebuliser gas flow, 0.9 l min^{-1}) was performed prior to each experiment. Very similar intensity values were obtained over the whole period of experimental work (RSD between 1.7 and 6.1%).

The reproducibility of the experimental protocol was also checked for the above conditions, by replicating the procedure three times. The three data sets obtained are comparable, particularly in terms of their characteristic drift patterns and the magnitude of the drift (Fig. 6).

The drift bias on each line and at every replicate was plotted for each set of conditions. These plots are presented in the Electronic Supplementary Information in the file.† Different drift patterns were found depending on the instrumental parameters, and also the magnitude of drift error varied with the instrumental settings. Some of the operating conditions produced very stable signals with drift values below 3% over the entire experiment, as was the case when using the central conditions, *i.e.*, rf power 1250 W and nebuliser flow rate 0.9 l min^{-1}, and the moderate conditions, rf power 1125 W and nebuliser flow rate 0.75 l min^{-1}. In other cases, the magnitude of the drift can reach values over 20%, *i.e.*, experimental conditions: rf power 1375 W, nebuliser flow rate 1.05 l min^{-1}. However, the most interesting observation from the results obtained is the evolution of the trends with the changes in the instrumental parameters. In Fig. 7, we have replaced each experimental point (described in Fig. 4) by a plot of the drift data set obtained at the corresponding experimental conditions. One can easily identify that some plots could be grouped together. For instance, in the right-bottom corner, the plots show two trends, one grouping all the analyte lines and the other containing the four argon lines. This was found under robust or at least moderately robust conditions: 1500 W, 0.60 l min^{-1}; 1375 W, 0.75 l min^{-1}; 1250 W, 0.60 l min^{-1} for

Table 6 Limit of detection of studied lines at different operating conditions (ppb). Figures in bold represent values which lie outside the 95% confidence interval

Experiment No.	CC	Ex. 1	Ex. 2	Ex. 3	Ex. 4	Ex. 5	Ex. 6	Ex. 7	Ex. 8	Ex. 9	Ex. 11	Ex. 12
Rf power/W	1250	1125	1125	1375	1375	1000	1250	1250	*1500*	1000	1500	1500
Nebuliser gas flow/l min^{-1}	0.9	1.05	0.75	1.05	0.75	0.9	1.2	0.6	0.9	1.2	1.2	0.6
Al - 396.152 - (I)	57	11	43	19	48	14	19	**170**	59	3	15	**140**
Ba - 230.424 - (II)	4	3	8	3	7	3	3	**22**	1.6	5	2	**20**
Ba - 233.527 - (II)	3	1.3	4	1.6	4	3	2	**13**	2	3	1.6	**23**
Ca - 317.933 - (II)	6	4	6	3	6	5	4	**35**	5	3	2	**60**
Ca - 422.673 - (I)	17	3	15	4	9	7	5	35	8	1.4	3	**120**
Cd - 226.502 - (II)	3	2	3	2	3	3	1.6	**10**	1.8	4	1.8	**14**
Cd - 228.802 - (I)	6	5	8	4	9	5	5	**20**	6	7	4	**31**
Co - 228.616 - (II)	11	9	25	7	15	15	7	**52**	8	6	4	**69**
Co - 340.512 - (I)	75	23	63	24	110	29	21	190	33	12	21	**840**
Cr - 267.716 - (II)	6	2	6	2	2	4	3	9	1.8	4	1.5	**33**
Cr - 357.869 - (I)	15	4	21	7	41	5	6	**100**	11	2	7	**240**
Cu - 224.700 - (II)	10	6	12	4	16	4	3	**45**	7	1.5	6	**65**
Cu - 324.754 - (I)	3	1.0	5	1.3	8	1.1	1.3	**26**	3	0.5	1.4	**45**
Fe - 259.940 - (II)	3	1.2	3	1.8	5	3	1.7	**13**	1.3	1.2	1.0	**19**
Mg - 279.079 - (II)	30	11	25	9	21	14	14	82	18	8	13	**260**
Mg - 280.270 - (II)	0.5	0.2	0.5	0.5	0.6	4	0.5	1.5	0.6	0.2	1.2	1.4
Mg - 285.213 - (I)	1.1	0.6	1.9	1.0	2	5	0.6	**6**	1.2	0.5	1.1	**13**
Mg 279.553 - (II)	0.6	0.3	0.4	0.5	0.6	**4**	0.5	0.8	0.5	0.2	1.1	**1.5**
Mn - 257.610 - (II)	0.6	0.3	1.2	0.3	0.6	0.4	0.3	**3**	0.6	0.3	0.3	**3**
Mn - 403.076 - (I)	120	14	56	44	55	19	23	**430**	130	4	20	**520**
Na - 589.592 - (I)	40	7	31	8	30	15	14	110	32	3	11	**360**
Ni - 231.604 - (II)	6	3	11	2	13	8	6	**32**	5	6	7	**64**
Ni - 232.003 - (I)	16	11	34	13	26	11	9	**69**	12	9	11	**77**
Pb - 216.999 - (I)	160	72	250	87	220	81	77	**520**	110	41	46	**690**
Pb - 220.353 - (II)	36	32	55	25	52	45	37	88	34	20	36	**230**
Ti - 337.280 - (II)	3	1.2	4	0.7	5	1.5	0.8	5	2	0.8	0.8	**17**
Zn - 202.548 - (II)	4	3	5	1.7	3	6	4	**12**	2	8	2	**16**
Zn - 213.856 - (I)	1.8	1.2	3	1.8	3	2	1.4	**6**	1.4	1.8	1.1	**6**

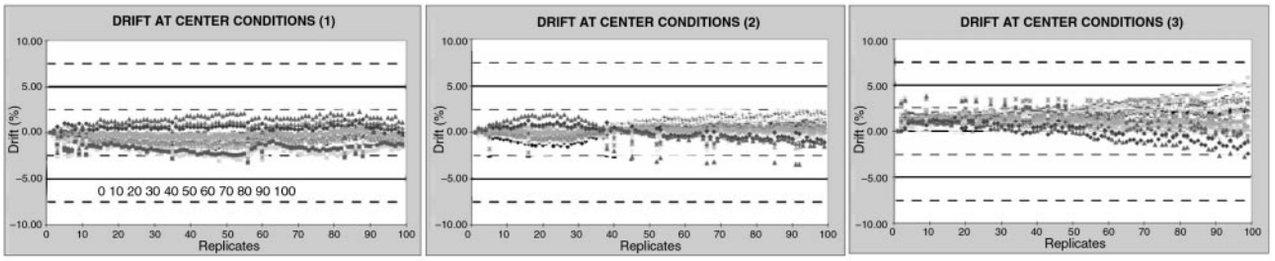

Fig. 6 Drift patterns at central conditions, three replicates: rf power, 1250 W and nebuliser gas flow, 0.9 l min^{-1}.

the rf power and the nebuliser gas flow rate, respectively. A deficiency in the transport system due to a low nebuliser flow may cause this separation between lines, since such conditions may lead to a partial blocking of the nebuliser tip, thus deteriorating its performance. This problem will only affect the analyte lines, while the argon lines, which are not necessarily involved in the nebulisation process, will remain unaffected.

Another set of similar patterns can be found in the right-top area of Fig. 7. This zone corresponds to unusual instrumental conditions, *i.e.*, high rf power and high nebuliser gas flow, and is therefore not of great practical interest. However, in a similar way to the results in the right-bottom area discussed above, two of the plots show similar trends. The experiments run at rf power 1375 W, nebuliser flow rate 1.05 l min^{-1} and at rf power 1500 W, nebuliser flow rate 1.20 l min^{-1} present similar patterns, with very unstable signals during half of the experiment prior to a stabilising of the signals.

In the middle area, near the central conditions, various plots show considerably robust data sets, with low drift values but relatively noisy signals, *i.e.*, the experimental settings 1250 W, 0.9 l min^{-1}; 1250 W, 1.2 l min^{-1} and 1125 W, 0.75 l min^{-1}. Under such conditions, no trends are observed and the evolution in the signal is quite chaotic.

A final group of plots can be recognised on the top left corner of Fig. 7. When using a low rf power and a high nebuliser gas flow (*i.e.*, 1000 W, 1.2 l min^{-1} or 1125 W, 1.05 l min^{-1}) a warming up effect is observed. Under such conditions, the plasma is slightly cooler due to the low power employed and the high setting for the nebuliser gas, which also contributes to the cooling effect. Finally, when setting the instrument at 1000 W and 0.9 l min^{-1}, *i.e.*, operating conditions which are very similar to the so called 'standard conditions', (1000 W and 1.0 l min^{-1}), high values of drift were observed. Under such settings, the emission signal drifts to progressively higher values.

Correlation and internal standardisation. The correlation coefficient is a measure of the linear relationship between fluctuations in the analyte and internal standard signals. Thus, to achieve a good drift correction by internal standardisation, high correlation between analyte lines and internal standards is necessary. In order to investigate the potential for internal

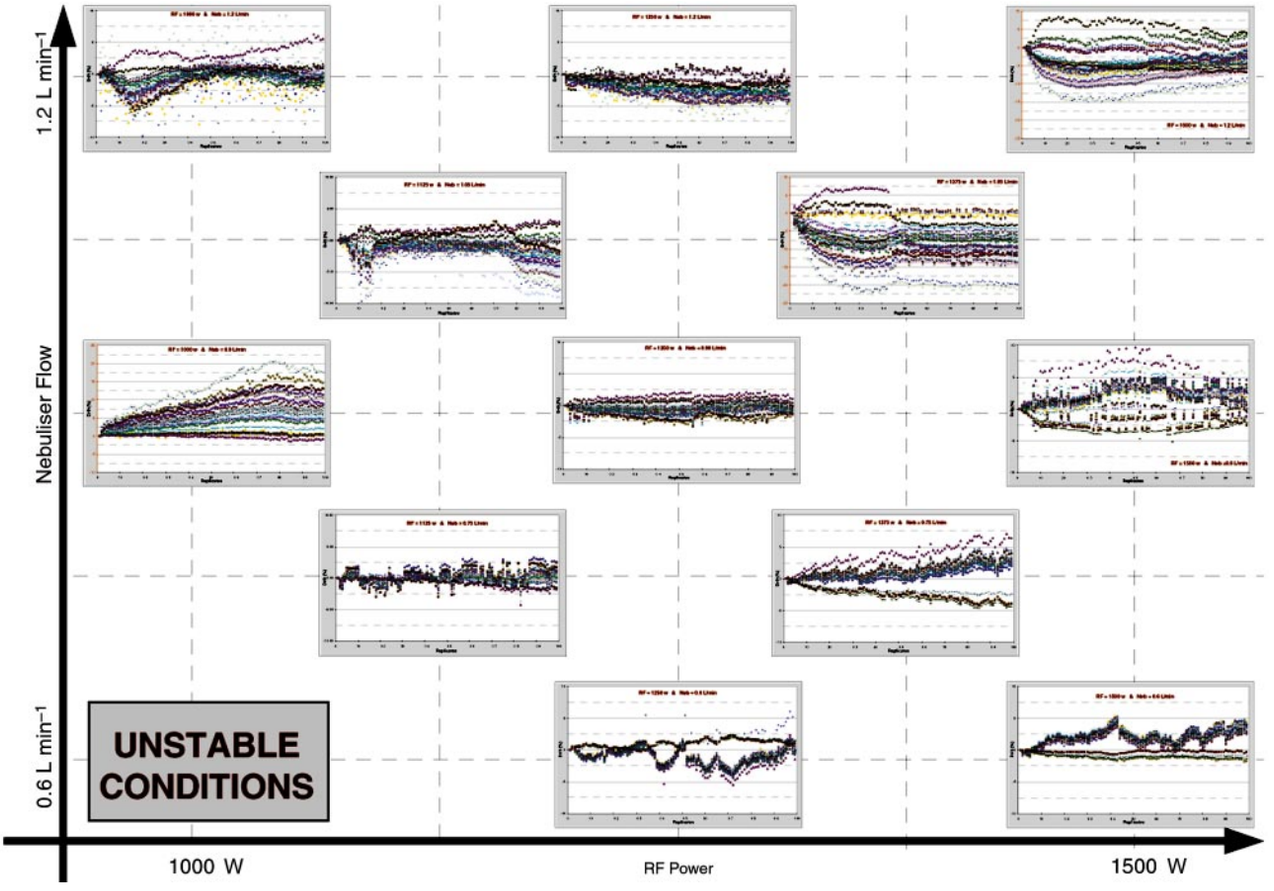

Fig. 7 Drift patterns at different experimental conditions. Details of the plots are available as Electronic Supplementary Information.†

Table 7 Summary of results

	Rf power/W	1000			1125		1250			1375		1500		
	Nebuliser flow rate/l min^{-1}	0.60	0.90	1.20	0.75	1.05	0.60	0.90	1.20	0.75	1.05	0.60	0.90	1.20
Drift after 8 h (%)	Average	—	7.32	1.14	1.08	3.20	0.53	0.87	2.89	3.17	8.89	3.47	2.18	3.75
	Minimum	—	0.24	0.02	0.02	0.12	0.07	0.01	0.49	1.98	0.11	0.35	0.01	0.36
	Maximum	—	17.46	5.59	2.59	9.01	1.48	1.61	5.79	6.45	21.17	8.83	4.56	9.79
Correlation[a]	Average	—	0.71	0.62	0.54	0.40	0.95	0.41	0.61	0.98	0.53	0.97	0.64	0.55
	Atomic–Atomic	—	0.58	0.58	0.44	0.18	0.91	0.35	0.50	0.98	0.39	0.97	0.68	0.36
Analyte–Analyte	Ionic–Ionic	—	0.89	0.69	0.83	0.88	0.98	0.61	0.86	0.98	0.77	0.97	0.66	0.91
	Atomic–Ionic	—	0.66	0.59	0.42	0.21	0.94	0.32	0.52	0.97	0.46	0.97	0.61	0.42
Correlation[a]	Average	—	0.79	0.70	0.54	0.40	−0.74	0.28	0.62	−0.87	0.63	−0.80	−0.05	0.28
	Argon–Atomic	—	0.64	0.62	0.23	0.04	−0.73	0.08	0.40	−0.89	0.52	−0.79	−0.06	0.09
Argon–Analyte	Argon–Ionic	—	0.92	0.76	0.80	0.71	−0.75	0.46	0.81	−0.86	0.72	−0.80	−0.04	0.44
Remarks	Trends	—	Yes	?	No	?	Yes	No	No	Yes	Yes	Yes	Yes	Yes

[a]Pearson's correlation.

standard methods to correct for long-term drift error at each of the operating conditions tested, the correlation matrices of each data set have been calculated. The correlation matrices are presented in the Electronic Supplementary Information in the file "CORR-MAT.doc".† These matrices quantify the similarities and differences observed from the drift plots in Fig. 7. Correlation between emission lines changes from one set of experimental conditions to another, as well as the type (*i.e.*, atomic, ionic, argon) of lines showing good correlation. Likewise, we only observed very high inter-analyte correlation when working at robust or moderately robust conditions, independent of the nature of the emission line, *i.e.*, atomic or ionic line. Table 7 summarises the information obtained by studying the correlation matrices.

The different patterns identified when varying the instrumental conditions highlight the difficulties when trying to optimise a general correction method for drift. The use of internal standardisation has been a common approach to minimise the drift from the early work of Barnett *et al.*[30,31] and Myers and Tracy[32] to more recent and complicated approaches.[7,33–40] Our results are in agreement with those of Romero *et al.*[9] and indicate that whilst internal standardisation may be an option when working under robust conditions, the approach is of very little value when softer settings are employed. Of particular interest is the possibility of correcting for drift by employing an argon line, as is the case when moderate robust conditions (rf power 1375 W, nebuliser flow rate 1.05 l min^{-1}) are employed.

Fig. 8 and Fig. 9 show the changes in the shape of the drift patterns before and after internal standardisation under two different operating conditions: rf power 1500 W, nebuliser flow

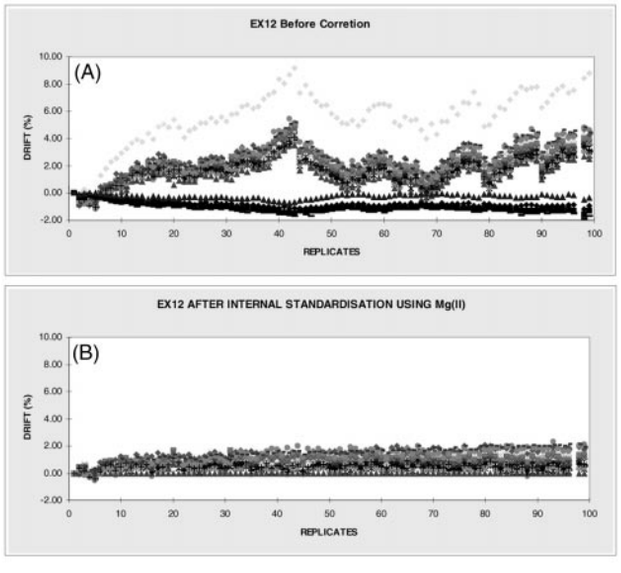

Fig. 8 Drift correction by internal standardisation using experimental conditions as for Experiment 12; rf power = 1500 W and nebuliser gas flow = 0.6 l min^{-1}. At robust conditions any analyte line can alleviate long term drift (example using MgII line). (A) Two groups of lines are observed, one containing all the analyte lines (on the top of the plot) and the other containing only the four argon lines. (B) When MgII is employed as internal standard, using $A_n^{\mathrm{corr}} = A_n + [(I_0 - I_n)/I_n] \times A_n$ which expects similar drift errors in the analyte line and internal standard line, most of the long-term noise is removed.

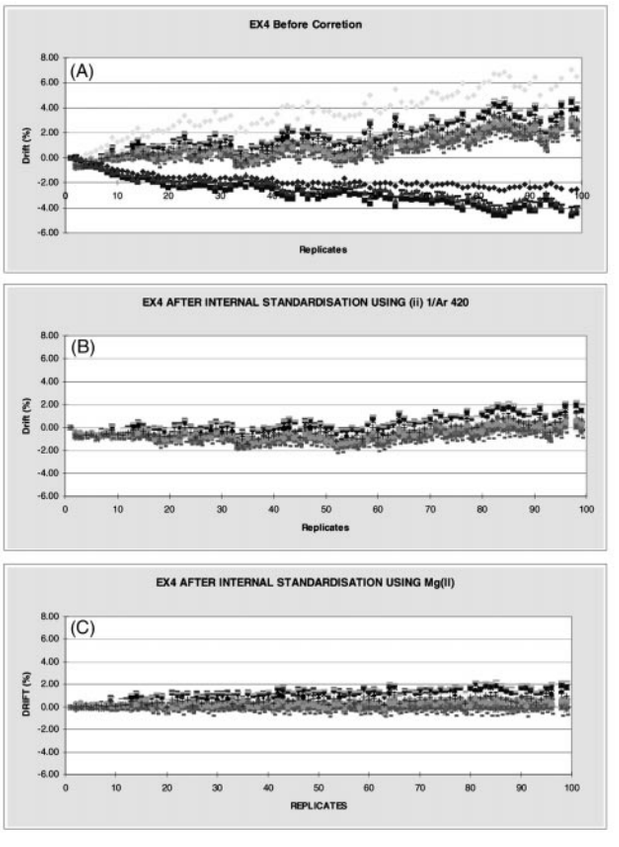

Fig. 9 Drift correction by internal standardisation using experimental conditions as in Experiment 4; rf power = 1375 W, nebuliser gas flow = 0.75 l min^{-1}. (A) Drift pattern before correction. High correlation between analyte lines is observed and the four argon lines. High negative correlation between both groups can be observed. (B) Drift on the analyte lines using the inverse of $Ar^{420.063\ nm}$ as an internal standard and using the formula $A_n^{\mathrm{corr}} = A_n - 0.5[(I_0 - I_n)/I_n] \times A_n$. The 0.5 factor was introduced to optimise the correction. (C) Drift on the analyte lines using the $Mg^{279.079\ nm}$ line as internal standard using the formula $A_n^{\mathrm{corr}} = A_n + [(I_0 - I_n)/I_n] \times A_n$.

Table 8 Improvement factors obtained when correcting drift by internal standardisation at robust conditions: rf power 1500 W, nebuliser gas flow rate 0.6 l min^{-1}

	Drift before correction (%)	Drift after correction by Mg (II) line (%)	Factor of improvement, IF
Al - 396.152 - (I)	3.04	0.55	5
Ba - 230.424 - (II)	4.02	1.51	3
Ba - 233.527 - (II)	4.05	1.54	3
Ca - 317.933 - (II)	2.89	0.41	7
Ca - 422.673 - (I)	3.89	1.38	3
Cd - 226.502 - (II)	4.16	1.65	3
Cd - 228.802 - (I)	3.89	1.39	3
Co - 228.616 - (II)	4.38	1.86	2
Co - 340.512 - (I)	2.89	0.41	7
Cr - 267.716 - (II)	3.55	1.06	3
Cr - 357.869 - (I)	2.76	0.28	10
Cu - 224.700 - (II)	4.27	1.76	2
Cu - 324.754 - (I)	3.58	1.08	3
Fe - 259.940 - (II)	3.89	1.38	3
Mg - 279.079 - (II)	2.47	0.10	25
Mg - 285.213 - (I)	3.05	0.57	5
Mn - 257.610 - (II)	3.70	1.20	3
Mn - 403.076 - (I)	3.56	1.06	3
Na - 589.592 - (I)	8.83	6.21	1
Ni - 231.604 - (II)	3.08	0.60	5
Ni - 232.003 - (I)	4.37	1.86	2
Pb - 220.353 - (II)	4.63	2.11	2
Ti - 379.280 - (II)	3.18	0.69	5
Zn - 202.548 - (II)	4.45	1.93	2
Zn - 213.856 - (I)	3.79	1.29	3

rate 0.6 l min^{-1} and rf power 1375 W, nebuliser flow rate 0.75 l min^{-1}. The improvement factors for each case are shown in Tables 8 and 9.

Multi-way analysis

From Fig. 7, the variation of the drift patterns from one set of conditions to another is not random. Groups of settings with similar drift patterns are observed, reflecting the progressive change in drift patterns when varying the instrumental conditions. The complete array of data as described in previous sections was analysed simultaneously by performing a parallel factor analysis.

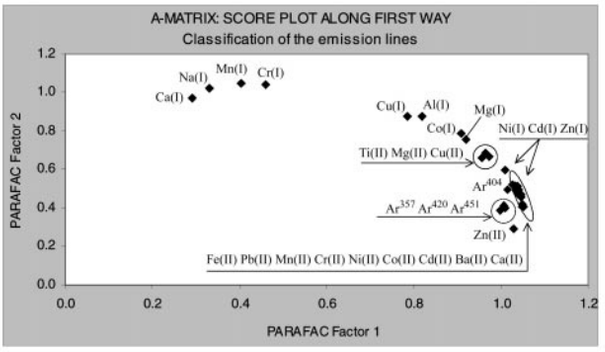

Fig. 10 PARAFAC score plot along the first mode.

The use of PARAFAC found that the best model resulted when only two factors were calculated (96.8% of the total variance was explained). Clearly, this was expected since we are altering just two instrumental parameters in this study, and it may indicate that the model is working well.

The "PARAFAC-score plots" have been plotted in Fig. 10. A partial separation can be noticed between atomic and ionic lines and especially between soft and hard lines. Closer to the right hand side bottom corner of the plot, *i.e.*, high score on PARAFAC factor 1 and low on PARAFAC factor 2, the emission line is the hardest. In a similar way, Fig. 11 represents the loadings of factor 1 and 2 along the second dimension *versus* replicates, *i.e.*, time. The drift patterns of some specific instrumental conditions have clearly conditioned the formation of theses factors.

Finally, Fig. 12 shows the PARAFAC loading plot along the third mode. The distribution of the experiment points on the new axes is nearly linear, with a remarkable trend to robust

Table 9 Improvement factors obtained when correcting drift by internal standardisation at moderately robust conditions: rf power 1375 W, nebuliser gas flow rate 0.75 l min^{-1}

	Drift before correction (%)	Drift after correction by Ar line (%)	Drift after correction by Mg (II) line (%)	Factor of improvement when using Ar IF	Factor of improvement when using Mg (II) IF
Al - 396.152 - (I)	3.0	0.6	0.8	5	4
Ba - 230.424 - (II)	2.6	0.3	0.5	10	5
Ba - 233.527 - (II)	2.3	0.0	0.2	80	11
Ca - 317.933 - (II)	2.2	−0.2	0.0	11	51
Ca - 422.673 - (I)	3.9	1.5	1.8	3	2
Cd - 226.502 - (II)	2.9	0.5	0.8	5	4
Cd - 228.802 - (I)	2.0	−0.4	−0.1	6	17
Co - 228.616 - (II)	2.8	0.4	0.7	7	4
Co - 340.512 - (I)	2.4	0.1	0.3	42	8
Cr - 267.716 - (II)	2.6	0.2	0.5	12	6
Cr - 357.869 - (I)	3.9	1.5	1.7	3	2
Cu - 224.700 - (II)	2.9	0.5	0.8	6	4
Cu - 324.754 - (I)	3.2	0.8	1.0	4	3
Fe - 259.940 - (II)	2.3	0.1	0.2	60	11
Mg - 279.079 - (II)	2.1	−0.2	0.1	9	21
Mg - 285.213 - (I)	2.1	−0.3	0.0	8	177
Mn - 257.610 - (II)	2.2	−0.2	0.1	13	27
Mn - 403.076 - (I)	4.4	2.0	2.2	2	2
Na - 589.592 - (I)	6.5	4.0	4.3	2	2
Ni - 231.604 - (II)	1.9	−0.5	−0.2	4	8
Ni - 232.003 - (I)	3.3	0.9	1.1	4	3
Pb - 220.353 - (II)	2.8	0.4	0.6	7	4
Ti - 379.280 - (II)	3.1	0.7	1.0	4	3
Zn - 202.548 - (II)	1.4	−0.9	−0.7	2	2
Zn - 213.856 - (I)	2.7	0.3	0.6	8	5

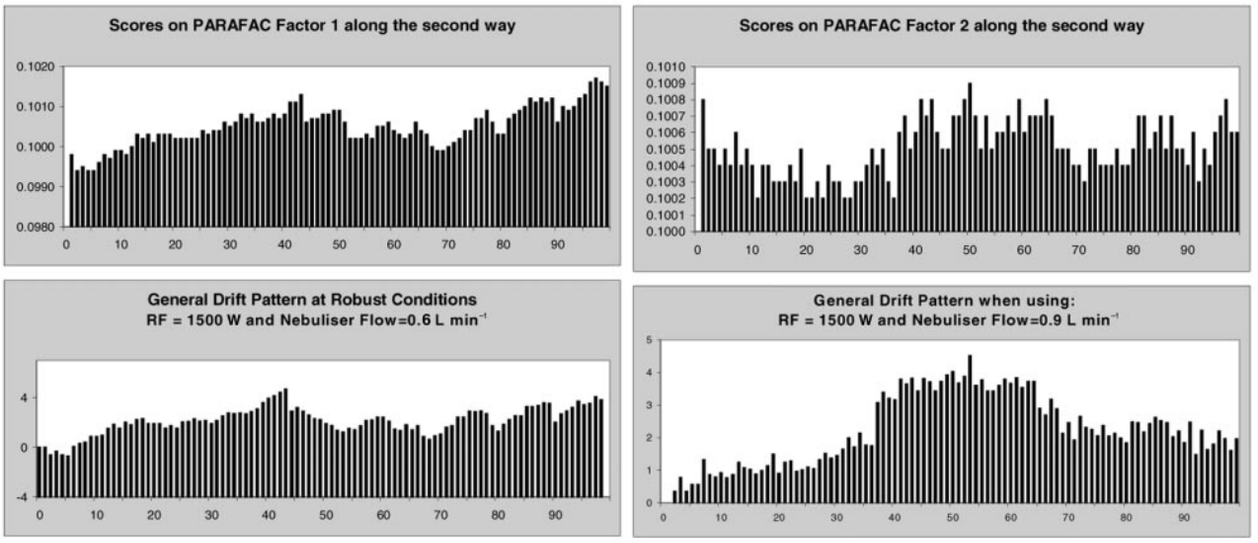

Fig. 11 PARAFAC factors along the second mode. Similarities to the drift patterns at some specific instrumental conditions.

conditions, *i.e.*, high rf power and low nebuliser gas flow rate. In order to quantify these graphic observations, the degree of correlation, r, between the loadings of the new PARAFAC factors and several physical parameters of our data has been calculated. Thus, the scores of the new components in the first mode (A-matrix) were correlated to the energy data of the lines studied: excitation energy, ionisation energy and emission energy of the monitored lines. The B-loading matrix was compared to the shape of the drift patterns, and the C-loadings were correlated to the levels of the rf power and the nebuliser flow rate set in each experiment. Importantly, the correlation levels found in this exercise enables the interpretation of the physical significance of the PARAFAC factors. The results are summarised below:

Within the 1st mode: emission lines. Factor 1: some correlation was found between the emission energy of the emission lines and the scores of PARAFAC factor 1, ($r = 0.58$). Factor 2: the scores of the second factor are highly correlated to the inverse of the excitation energy of the emission lines ($r = 0.90$).

Within the 2nd mode: replicates/time. Factor 1: the loadings of this factor are highly correlated to the general (average) analyte drift patterns at robust and moderately robust conditions ($r = 0.92$). Factor 2: some correlation was found ($r \approx 0.6$) between this factor and the average drift pattern when using 1500 W and 0.9 l min^{-1} and when using default conditions, 1000 W and 0.9 l min^{-1} (Fig. 11).

Within the 3rd mode: experimental conditions. Factor 1: the nebuliser gas flow rate employed in the different drift diagnoses was highly correlated to the loadings of PARAFAC factor 1 along the third mode ($r = 0.93$). Factor 2: the loadings of factor 2 were found very highly correlated ($r = 0.97$) to the ratio: (rf power)/(nebuliser flow rate).

It is important to note that although no analytical information was incorporated into the matrix when performing the PARAFAC analysis, the new factors are highly correlated to some of the physical parameters investigated. This strong association suggests that the two instrumental parameters modified in our study are related to the cause of most of the variation in the data set and so are intrinsic to the drift phenomenon.

Conclusions

The results presented here are in agreement with and complementary to previous work indicating that the rf power and the nebuliser gas flow rate settings have a fundamental effect on the robustness of the data.

The results shown in Fig. 7 could provide the analyst with a quick reference to better optimise instruments for long-term stability. In addition, this study facilitates the appropriate use of internal standards for drift correction. (1) Soft conditions, low power (rf power $\approx$ 1000 W) with medium to high nebuliser flow (> 1.0 l min^{-1}) give very unstable signals over time and complex drift patterns. Under these conditions, the use of an internal standard to compensate for instrument drift will not lead to an improvement on the quality of the data. For such conditions, the authors have developed a new correction procedure.[41] (2) With medium power (rf power = 1250 W), the data obtained indicate that the instrument is generally quite stable, showing drift values below 5% and complex drift patterns. Although drift correction under such conditions might be not necessary, internal standardisation methods will not be appropriate. (3) Under robust conditions, the instability is highly correlated between all the analyte lines and any line

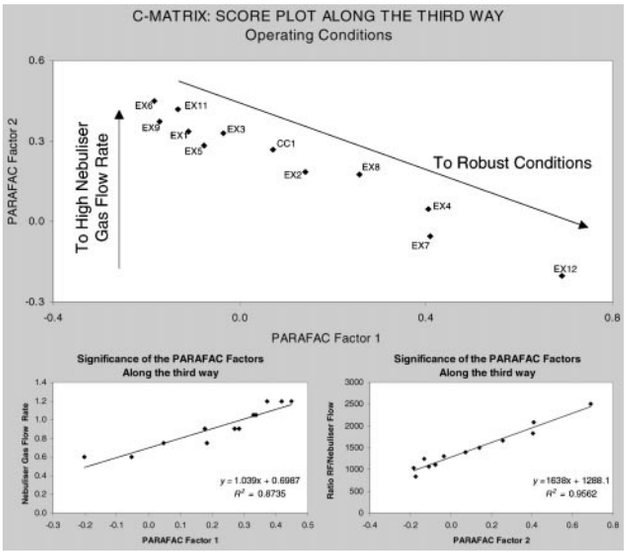

Fig. 12 PARAFAC score plot along the third mode. Physical interpretation of the model factors.

can be employed to correct for drift. Of specific interest are the so called "moderate robust conditions" (rf power 1375 W, nebuliser flow rate 1.05 l min^{-1}) where argon lines could be used as internal standards.

The use of the multi-way approach, PARAFAC, has also been shown to be a powerful tool to describe the system. The results are easier to interpret than those obtained using PCA due to the smaller number of parameters implied in the formation of the PARAFAC factors. A mathematically agreed interpretation of the tri-dimensional factors has been achieved by using physical parameters related to the system.

However, the full potential of this technique has not yet been realised and work in this area will continue, particularly in the area of multi-way regression[42] to correct for drift. Matrix effects and the influence of concentration levels on long-term stability of signals will also be the subject of further work.

Acknowledgements

The authors wish to acknowledge Dr. Mark Cave for support and inspiration, as well as the British Geological Survey (Keyworth, UK) and the University of Plymouth for financing this project.

References

1 S. J. Hill, *Inductively Coupled Plasma Spectrometry and its Applications*, Sheffield Academic Press, UK, 1999.
2 E. D. Salin and G. Horlick, *Anal. Chem.*, 1980, **52**, 1578.
3 R. M. Belchamber and G. Horlick, *Spectrochim. Acta, Part B*, 1982, **37**, 71.
4 R. M. Belchamber and G. Horlick, *Spectrochim. Acta, Part B*, 1982, **37**, 17.
5 M. H. Ramsey and M. Thompson, *Analyst*, 1985, **110**, 519.
6 M. Carre, E. Poussel and J. M. Mermet, *J. Anal. At. Spectrom.*, 1992, **7**, 791.
7 J. M. Mermet and J. C. Ivaldi, *J. Anal. At. Spectrom.*, 1993, **8**, 795.
8 G. J. Schmidt and W. Slavin, *Anal. Chem.*, 1982, **54**, 2491.
9 X. Romero, E. Poussel and J. M. Mermet, *Spectrochim. Acta, Part B*, 1997, **52**, 487.
10 J. M. Mermet, *Spectrochim. Acta, Part B*, 1989, **44**, 1109.
11 J. M. Mermet, *Anal. Chim. Acta*, 1991, **250**, 85.
12 A. Lopezmolinero, A. V. Caballero and J. R. Castillo, *Spectrochim. Acta, Part B*, 1994, **49**, 677.
13 A. K. Smilde, *Chemometrics and Intelligent Laboratory Systems*, 1992, **15**, 143.
14 R. Bro, *Chemometrics and Intelligent Laboratory Systems*, 1997, **38**, 149.
15 R. A. Harshman and M. E. Lundy, *Computational Statistics & Data Analysis*, 1994, **18**, 39.
16 A. C. Atkinson and A. N. Donev, *Optimum Experimental Designs*, Oxford Science Publications, UK, 1996.
17 D. C. Montgomery, *Design and Analysis of Experiments*, John Wiley & Sons, Chichester, UK, 1997.
18 B. G. M. Vandeginste, D. L. Massart, L. C. M. Buydens, S. DeJong, P. J. Lewi and J. Smeyers-Verbeke, *Handbook of Chemometrics and Qualimetrics*, Elsevier Science B. V, 1998.
19 R. A. Harshman, *UCLA Working Papers in Phonetics*, 1970, **16**, 1.
20 J. L. Beltran, R. Ferrer and J. Guiteras, *Anal. Chim. Acta*, 1998, **373**, 311.
21 R. Bro, *Chemometrics and Intelligent Laboratory Systems*, 1999, **46**, 133.
22 L. Norgaard, *J. Chemom.*, 1996, **10**, 615.
23 P. Hindmarch, K. Kavianpour and R. G. Brereton, *Analyst*, 1997, **122**, 871.
24 A. K. Smilde and D. A. Doornbos, *J. Chemom.*, 1991, **5**, 345.
25 R. Boque and A. K. Smilde, *AIChE Journal*, 1999, **45**, 1504.
26 K. S. Dahl, M. J. Piovoso and K. A. Kosanovich, *Chemometrics and Intelligent Laboratory Systems*, 1999, **46**, 161.
27 J. A. Westerhuis, T. Kourti and J. F. Macgregor, *J. Chemometr.*, 1999, **13**, 397.
28 J. L. Todoli and J. M. Mermet, *Spectrochim. Acta Part B*, 1999, **54**, 895.
29 The *N*-way toolbox for MATLAB, ver. 1.02, KVL, Denmark, 1999. http://newton.foodsci.kvl.dk/Matlab/nwaytoolbox/index.htm.
30 W. B. Barnett, V. A. Fassel and R. N. Kniseley, *Spectrochim. Acta Part B*, 1968, **23**, 643.
31 W. B. Barnett, V. A. Fassel and R. N. Kniseley, *Spectrochim. Acta Part B*, 1970, **25**, 139.
32 S. A. Myers and D. H. Tracy, *Spectrochim. Acta Part B*, 1983, **38**, 1227.
33 A. S. AlAmmar, H. A. Hamid and B. H. Rashid, *Spectrochim. Acta Part B*, 1990, **45**, 359.
34 A. Lorber, Z. Goldbart and M. Eldan, *Anal. Chem.*, 1984, **56**, 43.
35 A. Lorber and Z. Goldbart, *Anal. Chim. Acta*, 1984, **161**, 163.
36 A. S. AlAmmar and R. M. Barnes, *At. Spectrosc.*, 1998, **19**, 18.
37 M. H. Ramsey and M. Thompson, *Analyst*, 1984, **109**, 1625.
38 J. N. Walsh, *Chem. Geol.*, 1992, **95**, 113.
39 V. Kanicky, *Collection Czechoslovak Chem. Commun.*, 1993, **58**, 2905.
40 D. A. Sadler, F. Sun, S. E. Howe and D. Littlejohn, *Mikrochim. Acta*, 1997, **126**, 301.
41 A. Marcos and S. J. Hill, *Analyst*, 2000, **125**, 1015.
42 R. Bro, *J. Chemom.*, 1996, **10**, 47.